# The point spread function of optical microscopes imaging through stratified media

Olivier Haeberlé, Mehdi Ammar, Hiromitsu Furukawa, Koji Tenjimbayashi, Peter Török

# The point spread function of optical microscopes imaging through stratified media

**O. Haeberlé, M. Ammar**
*Groupe Lab.El – Laboratoire MIPS, Université de Haute-Alsace, 61 rue A. Camus F-68093 Mulhouse Cedex France*

**H. Furukawa, K. Tenjimbayashi**
*OptMec, Photonics Research Institute, AIST, Namiki 1-2, Tsukuba, Ibaraki 305-8564 Japan*

**P. Török**
*Blackett Laboratory, Imperial College London, Prince Consort Road, London SW7 2BW, UK*

**Abstract:** We propose a model for imaging point objects through a dielectric interface or stratified media. The model is applicable to conventional and confocal fluorescence microscopy, with single- or multi-photon excitation. An analytical solution is obtained in the form of readily computable functions. When large mismatches occur in the refractive indices of the media of the objective lens and specimen the illumination and detection point spread functions differ significantly, showing that currently used imaging models may fail to correctly predict imaging properties of optical microscopes.



**OCIS codes:** (260.0260) Physical optics; (180.0180) Microscopy; (050.1960) Diffraction theory

## References and links

1. F. Perrin, "La fluorescence des solutions," Ann. Phys. (Paris) **12**, 169-275 (1929)
2. P. Soleillet, "Sur les paramètres caractérisant la polarization partielle de la lumière dans les phénomènes de fluorescence," Ann. Phys. (Paris) **12**, 23-86 (1929)
3. D. Axelrod, "Carbocyanine dye orientation in red cell membrane studied by microscopi fluorescence polarization," Biophys. J. **26**, 557-574 (1979)
4. I. Gryczynski, H. Malak and J.R. Lakowicz, "Multiphoton excitation of the DNA stains DAPI and Hoechst," Bioimaging **4**, 138-148 (1996)
5. P. Török, P.D. Higdon, and T. Wilson, "On the general properties of polarized light conventional and confocal microscopes," Opt. Comm. **148**, 300-315 (1998)
6. P.D. Higdon, P. Török, and T. Wilson, "Imaging properties of high aperture multiphoton fluorescence scanning optical microscopes," J. Microsc. (Oxford) **193**, 127-141 (1999)
7. P. Török, P.D. Higdon and T. Wilson, "Theory for confocal and conventional microscopes imaging small dielectric scatterers," J. Mod. Opt. **45**, 1681-1698 (1998)
8. C.J.R. Sheppard and P. Török, "An electromagnetic theory of imaging in fluorescence microscopy, and imaging in polarization fluorescence microscopy," Bioimaging **5**, 205-218 (1997)
9. P. Török and P. Varga, "Electromagnetic diffraction of light focused through a stratified medium," Appl. Opt. **36**, 2305-2312 (1997)
10. P. Török, "Propagation of electromagnetic dipole waves through dielectric interfaces," Opt. Lett. **25**, 1463-1465 (2000)
11. Note that there was a typo in Eq. (6) and Eq. (14c) defining $\Psi_{det}$ in Ref. 10.
12. D. Minsky, "Memoir on Inventing the Confocal Scanning Microscope," Scanning **10**, p. 128-138 (1988)
13. S. Hell and E.H.K. Stelzer, "Fundamental improvement of resolution with a 4-Pi-confocal microscope using two-photon excitation," Opt. Comm. **93**, 277-281 (1992)
14. E. H. K. Stelzer and S. Lindek, "Fundamental reduction of the observation volume in far-field light microscopy by detection orthogonal to the illumination axis: confocal theta microscopy," Opt. Commun. **111**, p. 536-547 (1994)
15. O. Haeberlé *et al.*, "Multiple-objective microscopy with three-dimensional resolution near 100 nm and a long working distance," Opt. Lett. **26**, p. 1684-1686 (2001)

## 1. Introduction

Fluorescence microscopy is a key tool to study three-dimensional structures of living cells and tissues. When a fluorescent molecule is excited it essentially re-emits a dipole field [1-4], which is polarized. As a consequence, image formation models in fluorescence microscopy should take into account polarization effects.

The mathematical approaches proposed up to now [5-8] assume that an electric, magnetic or mixed dipole is excited by an electromagnetic wave and emits a perfect spherical wave. The limitation of these models is that they assume the dipole is embedded in a homogeneous medium, while in microscopy the specimen is often observed through an immersion medium and a cover glass whose refractive indices are usually different from that of the specimen.

In this work we present a rigorous model for image formation of fluorescent optical microscopes when a single fluorescent dipole is situated inside a stratified medium. The illumination of the dipole is modeled by the theory described in Ref [9]. The fluorescent dipole then emits a perfect dipole wave that traverses the stratified medium, as described in Ref [10]. A high numerical aperture lens collects and re-collimates light exiting the stratified medium. The evolution of the electric field vector is modeled by the generalized Jones matrix formalism [5]. A low convergence angle lens focuses the light emerging from the high aperture lens onto the detector. The image is built up by scanning the fluorescent dipole with respect to the illumination and detection systems. Note that this excitation mechanism corresponds to Case C of Ref [6].

Our approach therefore combines both stratified illumination and stratified detection in a vectorial model valid for conventional, confocal or multi-photon fluorescence microscopy.

## 2. Modeling of the illumination Point Spread function

Figure 1(a) shows the configuration for illumination by an *x*-polarized wave through a lens and a three-layer medium, which corresponds to the most common use of a fluorescence microscope, when the specimen is observed through an immersion medium and a cover glass. The first interface, perpendicular to the optical *z* axis, is placed at $z=-h_1$, the second interface at $z=-h_2$. The wave numbers of the specimen, cover glass and immersion medium are $k_3$, $k_2$ and $k_1$, respectively. In what follows we give generalized formulae for an *N*-layer medium and specialize the expressions later. ***E*** in italic describes the electric field in the focal region.

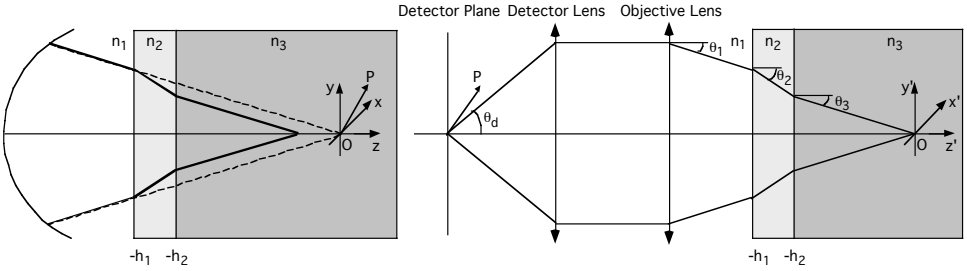


Fig. 1: (a) Focusing of an electromagnetic wave through a three-layer stratified medium. The origin *O* of the (*x*, *y*, *z*) reference frame is at the unaberrated Gaussian focal point. (b) Dipole radiation imaged through the same medium. The dipole is placed at the origin O of the (*x*', *y*', *z*') reference frame. Superscripts 1, 2, 3, and d are for the three media and the detector region.

The fluorescent molecule located at $P=(\rho,\phi,z)$, using the usual polar coordinate system notation, is excited by the focused wave. It then irradiates as a harmonically oscillating dipole, which moment $\boldsymbol{p}_e$ is co-polarized with the electric field ***E*** of Cartesian components [9]:

$$E_{Nx} = -i(I_{0ill} + I_{2ill}\cos 2\phi) \tag{1a}$$

$$E_{Ny} = -iI_{2ill}\sin 2\phi \tag{1b}$$

$$E_{Nz} = -2I_{1ill}\cos\phi \tag{1c}$$

$$I_{0ill} = \int_0^{\alpha_1} (\cos\theta_1)^{1/2}\sin\theta_1 J_0(k_1\rho\sin\theta_1)(T_s + T_p\cos\theta_N)\exp(ik_0\Psi_{ill})\exp(ik_N z\cos\theta_N)d\theta_1 \tag{2a}$$

$$I_{1ill} = \int_0^{\alpha_1} (\cos\theta_1)^{1/2}\sin\theta_1 J_1(k_1\rho\sin\theta_1)T_p\sin\theta_N\exp(ik_0\Psi_{ill})\exp(ik_N z\cos\theta_N)d\theta_1 \tag{2b}$$

$$I_{2ill} = \int_0^{\alpha_1} (\cos\theta_1)^{1/2}\sin\theta_1 J_2(k_1\rho\sin\theta_1)(T_s - T_p\cos\theta_N)\exp(ik_0\Psi_{ill})\exp(ik_N z\cos\theta_N)d\theta_1 \tag{2b}$$

$$\Psi_{ill} = h_{N-1}n_N\cos\theta_N - h_1 n_1\cos\theta_1 \tag{3}$$

In the above expression $\alpha_i$ is the convergence semi-angle of the illumination and $J_n(x)$ are the Bessel function order n, first kind. In Eq. (1), spherical polar coordinates are used with the usual notation $0 \le \theta \le \pi$ and $0 \le \phi < 2\pi$. The transmission coefficients $T_S$ and $T_p$ for the stratified medium are computed as in Ref [9].

### 3. Modeling of the detection Point Spread function

We consider now a ($x$', $y$', $z$') reference frame centered at the location of the molecule (see Fig. 1(b)). The electric field ***E*** emitted by the fluorescence process traverses back the stratified medium and is written before the objective lens (in medium 1) as [10]:

$$\begin{aligned} E_{1x'} = \frac{1}{2}\Big[ & p_{ex}^*(T_s' + T_p'\cos\theta_N\cos\theta_1) - 2p_{ez}^* T_p'\sin\theta_N\cos\theta_1\cos\phi_1 \\ & -(T_s' - T_p'\cos\theta_N\cos\theta_1)(p_{ex}^*\cos 2\phi_1 + p_{ey}^*\sin 2\phi_1)\Big] \end{aligned} \tag{4a}$$

$$\begin{aligned} E_{1y'} = \frac{1}{2}\Big[ & p_{ey}^*(T_s' + T_p'\cos\theta_N\cos\theta_1) - 2p_{ez}^* T_p'\sin\theta_N\cos\theta_1\sin\phi_1 \\ & -(T_s' - T_p'\cos\theta_N\cos\theta_1)(p_{ex}^*\sin 2\phi_1 - p_{ey}^*\cos 2\phi_1)\Big] \end{aligned} \tag{4b}$$

$$E_{1z'} = \Big[ p_{ez}^* T_p'\sin\theta_N\sin\theta_1 - T_p'\cos\theta_N\sin\theta_1(p_{ex}^*\cos\phi_1 + p_{ey}^*\sin\phi_1)\Big] \tag{4c}$$

Note that $(p_{ex}^*, p_{ey}^*, p_{ez}^*)$ now denotes the Cartesian components of the complex conjugate of ***p***. The transmission coefficients $T_S'$ and $T_p'$ for the stratified medium are computed as in Ref [9] but for propagation from medium $N$ towards medium 1, i.e. in the opposite sequence as for the illumination. When the dipole is imaged only part of the electromagnetic field given by Eq. (4) is collected and subsequently collimated by the objective lens. The electric vector **E** (upright **E** denotes the electric field after the lens) being collimated by the lens is given by:

$$\mathbf{E} = (\cos\theta_1)^{-1/2}\mathbf{R}^{-1}\cdot\mathbf{L}^{-1}\cdot\mathbf{R}\cdot E_1 \tag{5}$$

where the factor $(\cos\theta_i)^{-1/2}$ results from an inverse spherical-planar projection due to an aplanatic lens. The matrix **R** describes the coordinate transformation for rotation around the $z$-axis and the matrix **L** describes the change in the electric field as it traverses the lens [5]. Equation (5) leads to the Cartesian components of the electric vector field after the lens:

$$\begin{aligned} E_{x'} = \cos^{-1/2}\theta_1\Big\{ & p_{ex}^*\Big[(T_s' + T_p'\cos\theta_N) - (T_s' - T_p'\cos\theta_N)\cos 2\phi_1\Big] \\ & - p_{ey}^*(T_s' - T_p'\cos\theta_N)\sin 2\phi_1 - 2p_{ez}^* T_p'\sin\theta_N\cos\phi_1)\Big\} \end{aligned} \tag{6a}$$

$$\mathrm{E}_{y'} = \cos^{-1/2}\theta_1\Big\{-p_{ex}^{*}(T_s' - T_p'\cos\theta_N)\sin 2\phi_1 + p_{ey}^{*}\Big[(T_s' + T_p'\cos\theta_N) + (T_s' - T_p'\cos\theta_N)\cos 2\phi_1\Big] - 2p_{ez}^{*}T_p'\sin\theta_N\sin\phi_1)\Big\} \tag{6b}$$

$$\mathrm{E}_{z'} = 0 \tag{6c}$$

The detector lens serves as the second element of an aplanatic system, and is used to focus the electric field onto the detector. In order to achieve high overall magnification the numerical aperture of this lens is sufficiently low. We can thus simplify the model by stating that this lens produces in the back focal plane a truncated Fourier transform of the individual field components of the field in the front focal plane. Note that a more accurate representation was discussed in Ref. [7]. Hence:

$$\mathsf{E}_{x'} = FT(\mathrm{E}_{x'}) = p_{ex}^{*}(I_{0\,\mathrm{det}} + I_{2\,\mathrm{det}}\cos 2\phi_d) + p_{ey}^{*}(I_{2\,\mathrm{det}}\sin 2\phi_d) - 2iI_{1\,\mathrm{det}}p_{ez}^{*}\cos\phi_d \tag{7a}$$

$$\mathsf{E}_{y'} = FT(\mathrm{E}_{y'}) = p_{ex}^{*}I_{2\,\mathrm{det}}\sin 2\phi_d + p_{ey}^{*}(I_{0\,\mathrm{det}} - I_{2\,\mathrm{det}}\cos 2\phi_d) - 2iI_{1\,\mathrm{det}}p_{ez}^{*}\sin\phi_d \tag{7b}$$

with the quantities $I_{0\mathrm{det}}$, $I_{1\mathrm{det}}$ and $I_{2\mathrm{det}}$ defined as:

$$I_{0\,\mathrm{det}} = \int_0^{\alpha_d} (\cos\theta_1)^{-1/2}\sin 2\theta_d J_0(k_d\rho'\sin\theta_d)(T_s' + T_p'\cos\theta_3) \times \exp(-ik_0\Psi_{\mathrm{det}})\exp(-ik_1z'\cos\theta_1)d\theta_d \tag{8a}$$

$$I_{1\,\mathrm{det}} = \int_0^{\alpha_d} (\cos\theta_1)^{-1/2}\sin 2\theta_d J_1(k_d\rho'\sin\theta_d)\,T_p'\sin\theta_3 \times \exp(-ik_0\Psi_{\mathrm{det}})\exp(-ik_1z'\cos\theta_1)d\theta_d \tag{8b}$$

$$I_{2\,\mathrm{det}} = \int_0^{\alpha_d} (\cos\theta_1)^{-1/2}\sin 2\theta_d J_2(k_d\rho'\sin\theta_d)(T_s' - T_p'\cos\theta_3) \times \exp(-ik_0\Psi_{\mathrm{det}})\exp(-ik_1z'\cos\theta_1)d\theta_d \tag{8c}$$

with $\alpha_\mathrm{d}$ being the angular aperture of the detector lens, (r',z') are the radial and axial displacement of the dipole and the azimuthal angle $\theta_\mathrm{d}$ is related to the azimuthal angle $\theta$ by the relationship:

$$\frac{k_1\sin\alpha_1}{k_d\sin\alpha_d} = \frac{k_1\sin\theta_1}{k_d\sin\theta_d} = \beta \tag{9}$$

where $\beta$ is the nominal magnification of the detector lens system, and $k_\mathrm{d}$ is the wave number in the image space. The initial aberration function $\Psi_{\mathrm{det}}$ is given by [11]

$$\Psi_{\mathrm{det}} = n_1h_1\cos\theta_1 - n_Nh_{N-1}\cos\theta_N \tag{10}$$

The detected intensity is then obtained as:

$$PSF_{\mathrm{det}}(x',y',z') = \left|\mathsf{E}_{x'}\right|^2 + \left|\mathsf{E}_{y'}\right|^2 \tag{11}$$

Note that Eq. (8) differs from Eq. (2) in that now the inverse apodisation term is used and also that the transmission coefficients are different.

The model presented above is generally valid for scanning optical microscopes, including confocal microscopes. To specialize the results for a conventional microscope, a low numerical aperture condenser is used to produce an illumination with uniform lateral distribution. A simplified model then gives the resulting point spread function (PSF) by taking $\boldsymbol{p}_\mathrm{e}$ constant in modulus, and by averaging Eq. (11) over all dipole orientations [8], considering that the dipole is free to rotate, as is the case for example when the sample is in solution. In

that case Eq. (11) simplifies to $PSF_{det} = |I_{0det}|^2 + 2|I_{1det}|^2 + |I_{2det}|^2$. One may also consider polarized detection if a linear polarizer is introduced before the detector lens [5-8].

If one considers that the dipole is excited by a tightly focused beam then our model is specialized to confocal microscopy [12]. A first approximation is to consider randomly polarized fluorescent emission, and randomly polarized illumination. In that case one obtains $PSF_{conf} = PSF_{ill}\, PSF_{det} = \{|I_{0ill}|^2 + 2|I_{1ill}|^2 + |I_{2ill}|^2\}\{|I_{0det}|^2 + 2|I_{1det}|^2 + |I_{2det}|^2\}$. However, in previous works the detection PSF and illumination PSF were considered identical. The Fresnel transmission coefficients, however, are very different for propagation from e.g. water to glass or from glass to water. Hence for the case of focusing through a stratified medium the illumination and detection PSFs should be different even when computed for the same wavelength. A more precise approach is to compute the excitation PSF using Eqs. (1-3). Then the electric dipole moment, proportional to the $n^{th}$-power of the incident intensity for an $n$-photon fluorescence process, is obtained which permits an accurate calculation of the detected intensity. We note that our approach may also be useful for accurate modeling of multi-objective microscopes [13-15]

## 4. Results

Figure 2(a) shows the illumination PSF as given by Eqs. (1-3) and the detection PSF for a conventional microscope from Eqs. (7-11), along the optical $z$ axis, assuming $\boldsymbol{p}_e$=**const**= $p_{ex}\mathbf{i}_x$, for a dipole immersed in a watery medium, 50 μm below a 120 μm thick cover glass of refractive index 1.525, and for a 40x, N.A.=0.9 (air) objective lens [9]. The origin is at the position of the unaberrated gaussian focus point [16]. The objective lens is corrected for 170 μm cover glass thickness. For comparison, the illumination and detection PSFs are both computed for λ=488 nm. Aberrations are fairly well corrected in this case and the differences between the illumination and detection PSF are marginal. Figure 3(b) presents the resulting PSFs for the same system and a 170 μm thick cover glass. Note that in this case the PSFs exhibit strong spherical aberration. Furthermore, on comparing the illumination and detection PSFs noticeable differences appear suggesting that the usual approximation, which consists in assuming the illumination and detection PSFs identical, is not always valid. This is confirmed in Figure 3(c,d), which present the confocal PSFs corresponding to Figs. 3(a,b), computed using the usual approximation, and with our new dipole model. For single photon fluorescence the electric dipole moment is proportional to the illumination intensity, $p_e \propto |E|^2$, as given by Eqs. (1)-(3).

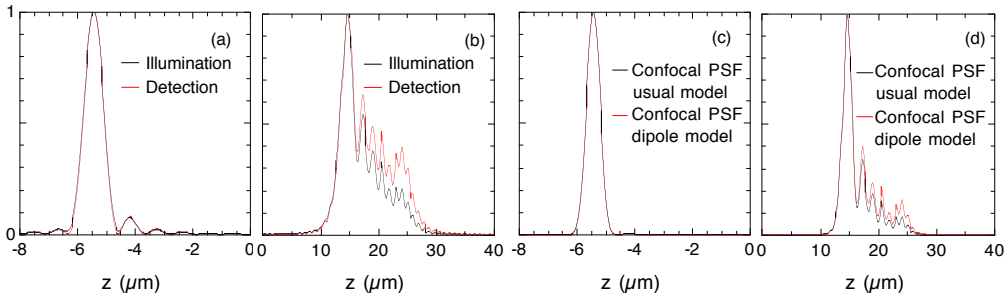


Fig. 2: Illumination and detection PSF at λ=488 nm with a 40x, N.A.=0.9 dry objective, for a single fluorescent molecule located in a watery medium 50 μm below (a): a 120 μm thickness cover glass and (b): a 170 μm thickness cover glass. (a) and (b) are for a conventional microscope. (c) and (d): confocal PSFs computed with the usual model and our dipole model. Figures (c) and (d) correspond to the same conditions as (a) and (b), respectively.

It is instructive to also consider the case of a dry objective lens which, due to the large difference between the refractive indexes of air and glass, represents the worst case scenario in terms of aberrations. Indeed, our results show that for oil immersion objectives the

difference between illumination and detection PSFs is weak. This is due to the small difference between the Fresnel coefficients corresponding to the illumination and detection PSFs, resulting from a fairly good match of refractive indexes. Figure 3(a) shows the illumination and detection PSFs, computed at λ=633 nm for a 63× oil immersion objective lens of N.A.=1.2, at a depth of 50 μm below a 170 μm cover glass, and for a conventional microscope. The two PSFs practically overlap each other in the main peak, with small differences in the tail.

For water immersion objective, and if the index of refraction of the specimen is considered to be exactly that of water, the illumination and detection PSF are identical, because the Fresnel coefficients are the same in both directions of propagation.

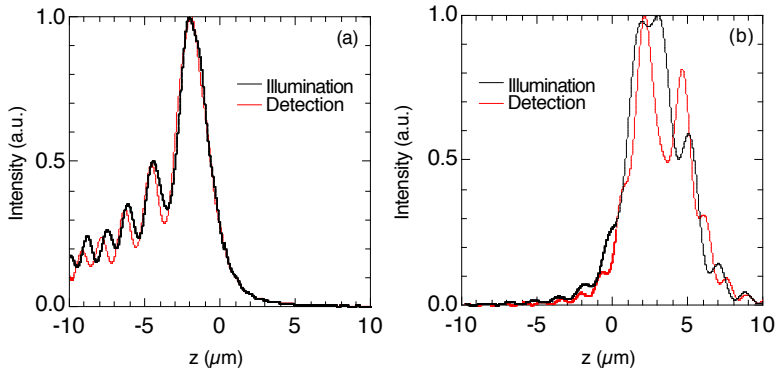


Fig. 3: (a) Illumination and detection PSF for a single fluorescent molecule located in a watery medium 50 μm below a 170 μm thickness cover glass, using a 63x oil immersion objective lens ($n_{oil}$=1.515) with N.A.=1.2 with both detection and illumination wavelength at 633 nm. (b) Illumination and detection PSF at 46.5 μm into diamond ($n_{spec}$=2.418). Both detection and illumination wavelengths are at 633 nm, using a 40x air immersion objective lens of N.A.=0.9. In the latter case the curves are very different, in contrast with the former case. Click panels to view movies of the PSFs as function of the observation depth (2.3 Mbyte each). Figures hold for a conventional microscope.

This result could be derived from the Helmholtz reciprocity theorem, and as a consequence, the so-called equivalence theorem holds in that case. In the general case, when mediums with different indexes of refraction are used, this theorem is not strictly valid, even if only small differences are expected (Fig. 3(a)). Therefore, considering the detection and illumination PSFs being identical for practical biological configurations is a fair approximation.

Conversely, when large mismatches of refractive index exist the use our new model seems essential. As an illustration, we consider crystallographic observation of diamond (n=2.418 at λ=633 nm) using a 40x dry objective lens of N.A.=0.9. Figure 3(b) shows the illumination and detection PSFs at a depth of 46.5 μm below the crystal surface and it is clear that large differences are observed.

The associated multimedia files show the PSFs as function of the focusing depth. Note the large differences, and also the fact that the peak of maximum intensity is often at a different location for the illumination and the detection PSFs in diamond, while for the oil immersion objective, both PSFs are very similar.

## 5. Conclusions

In conclusion we have presented a high aperture electromagnetic model for the image formation of fluorescence microscopes. The model is equally valid for conventional and confocal microscopy. When large refractive index mismatches occur our results show that the illumination and detection point spread functions of an optical microscope imaging a fluorescent molecule can significantly differ. This in turn results in an overall confocal point

spread function, which may be markedly different than that obtained from currently used models.

**Acknowledgements**

This work was supported by the New Energy and Industrial Technology Development Organization (NEDO) of Japan under an Industrial Technology Research Grant Program and the European Union within the framework of the Future and Emerging Technologies - SLAM program. Special thanks to B. Colicchio for the preparation of the multimedia files.